This is a repository copy of *Layered double hydroxide-derived copper-based oxygen carriers for chemical looping applications: oxygen release kinetics and impact of loading on long-term performance*.

White Rose Research Online URL for this paper:
https://eprints.whiterose.ac.uk/198377/

Version: Published Version

**Article:**

High, M., Song, Q., Campbell, K.L.S. et al. (1 more author) (2023) Layered double hydroxide-derived copper-based oxygen carriers for chemical looping applications: oxygen release kinetics and impact of loading on long-term performance. Greenhouse Gases: Science and Technology. ISSN 2152-3878

https://doi.org/10.1002/ghg.2214

# Layered double hydroxide-derived copper-based oxygen carriers for chemical looping applications: Oxygen release kinetics and impact of loading on long-term performance

**Michael  High and Qilei  Song**, Department of Chemical Engineering, Imperial College London, London, UK

**Kyra L. Sedransk  Campbell**, Department of Chemical and Biological Engineering, University of Sheffield, Sheffield S1 3JD, UK

**Paul S.  Fennell**, Department of Chemical Engineering, Imperial College London, London, UK

Abstract:  Chemical looping with oxygen uncoupling, a variant of chemical looping combustion, requires chemically and physically stable oxygen carriers over long-term redox cycling. Copper-based oxygen carriers are characterised by high oxygen release rates but experience sintering at high temperatures. The use of layered double hydroxides (LDHs), prepared *via* co-precipitation, as oxygen carrier precursors has been shown to effectively limit deactivation of copper-based mixed metal oxides (MMOs) over extended redox cycling. The LDH-derived MMOs have highly dispersed metal oxide within a stable support; the high dispersion of metals is due to the LDH precursor structure. In this work, a fluidised bed reactor (FBR) was used to study the intrinsic kinetics of oxygen release from $CuO/MgAl_2O_4$ oxygen carriers synthesised *via* the LDH-MMO design strategy. The long-term performance of MMOs with higher loadings of CuO, calcined from LDHs with higher Cu contents, was also investigated using an FBR. The intrinsic kinetics were determined using a kinetic model incorporating an effectiveness factor. By minimising the effects of intra- and inter-particle mass transfer, the activation energy and the pre-exponential factor of the lower loading MMOs were determined to be $51 \pm 3$ kJ mol$^{-1}$ and 0.0567 s$^{-1}$, respectively. All MMOs showed excellent stability over 100 redox cycles in a thermogravimetric analyser. However, the pH during co-precipitation of the LDHs affected the stability of the MMOs in an FBR. The MMOs calcined from LDHs synthesised at pH 9.5 disintegrated during operation, whilst those produced from LDHs synthesised at pH 11 maintained high

conversion and physical integrity over 100 redox cycles. © 2023 The Authors. *Greenhouse Gases: Science and Technology* published by Society of Chemical Industry and John Wiley & Sons Ltd.

*Additional supporting information may be found online in the Supporting Information section at the end of the article.*

# Introduction

Anthropogenic $CO_2$ emissions from fossil fuel combustion are a primary driver of climate change. Amongst next-generation CCUS technologies, chemical looping processes have attracted significant attention for inherent $CO_2$ capture without a significant energy penalty.[1] Chemical looping combustion (CLC) use oxygen carriers, commonly derived from transition metal oxides, to provide oxygen for combustion through cyclic redox reactions. The use of solid fuels (*e.g.*, biomass) for CLC typically requires a gasifying agent to overcome the slow solid–solid reactions between the solid char and oxygen carrier.[2] Chemical looping with oxygen uncoupling (CLOU) is a variant of CLC that was developed to overcome this issue and improve the $CO_2$ capture efficiency.[3] The technology uses oxygen carriers with suitable thermodynamics to release gaseous oxygen at high temperatures. The gaseous oxygen can react directly with the solid fuel through comparatively faster solid-gas reactions.

Oxygen carriers must maintain their performance over many cycles without chemical or mechanical deterioration for large-scale deployment of chemical looping processes. Suitable candidates for CLOU contain Cu, Mn and Co, either as single or mixed metal oxides (MMOs).[3,4] Employing Cu-based oxides is desirable to capitalise on Cu's oxygen uncoupling properties (high oxygen release capacity (0.101 $g_{O2}/g_{CuO}$) and fast oxygen release kinetics[5]). Two serious drawbacks of including Cu are the sintering and agglomeration behaviours which occur at high temperatures.[6] To improve the mechanical stability of the CuO oxygen carriers, $Al_2O_3$ is often used as a support.[7] One concern is that, over extended redox cycling active CuO can react with $Al_2O_3$ to form $CuAl_2O_4$.[8] This unintended product reduces the performance of the oxygen carrier because the rate of oxygen release from $CuAl_2O_4$ is much slower than from CuO at high temperatures.[9] Incorporating Mg into the Cu-Al system has been shown to stabilise the oxygen release capacity by inhibiting the formation of $CuAl_2O_4$ through the preferential formation of a $MgAl_2O_4$ support phase.[10,11]

We previously reported the synthesis of layered double hydroxide (LDH) precursors and calcined MMOs for chemical looping processes.[11–13] LDHs are a class of two-dimensional nanostructured anionic clays represented by the general formula $[(M^{2+})_{1-x}(M^{3+})_x(OH)_2]^{x+}(A^{n-})_{x/n} \cdot yH_2O$, where $M^{2+}$ are metal cations, for example, $Ca^{2+}$, $Cu^{2+}$, $Fe^{2+}$, $Mg^{2+}$, $Mn^{2+}$, $Ni^{2+}$, $Zn^{2+}$, etc., $M^{3+}$ could be *e.* $Al^{3+}$, $Fe^{3+}$, $Mn^{3+}$, *etc.*, and $A^{n-}$ is an interlayer anion, for example, $OH^-$, $CO_3^{2-}$ $NO_3^-$, $Cl^-$, etc. In our previous work, the Cu-Mg-Al LDH precursors were synthesised via co-precipitation using a 3:1:2 molar ratio of $Cu^{2+}:Mg^{2+}:Al^{3+}$.[11] Highly dispersed MMOs with a CuO loading of 63 wt% dispersed in a $MgAl_2O_4$ support were formed upon calcination of the LDH precursor (Fig. 1). The Cu-Mg-Al MMOs were tested in a fluidised bed reactor (FBR) and maintained a high performance over 100 cycles of complete oxygen release and oxygen storage.

Accurate knowledge of the intrinsic kinetics of the oxygen release reaction is required for the design of reactors for CLOU. However, these can be difficult to obtain due to errors in fitting traditional models to experimental data masked by external and internal mass transfer effects. In this work, the intrinsic oxygen release kinetics of the LDH-derived 3:1:2 Cu-Mg-Al MMOs were investigated using an FBR. The kinetics were extracted using a modified effectiveness factor-based model developed to study high-temperature CLC kinetics[14] and used to investigate the kinetics of CaO carbonation at elevated pressures.[15]

The oxygen release capacity determines the amount of oxygen that an oxygen carrier system can deliver. A larger solids inventory is required to fully convert the
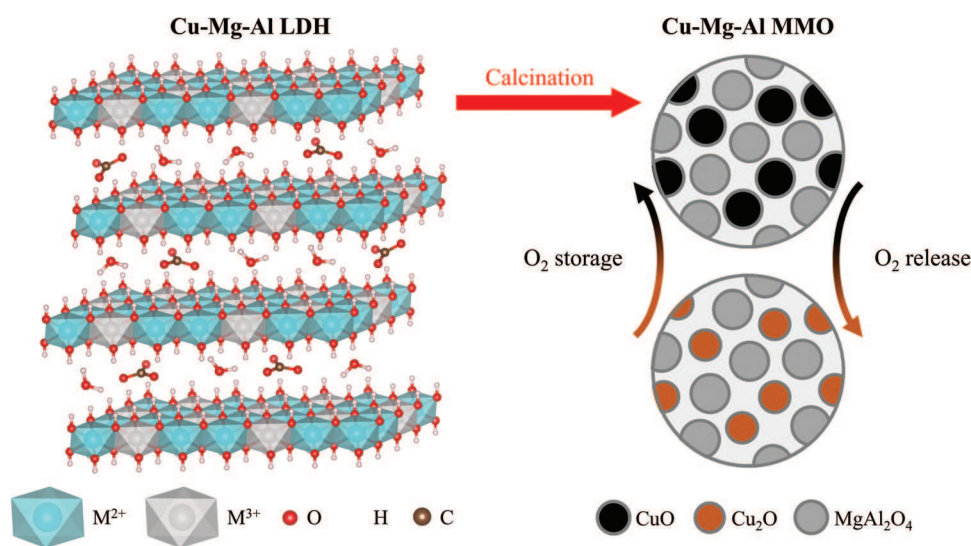
Figure 1. Cu-Mg-Al LDH-MMO design strategy (left to right): idealised structure of Cu-Mg-Al LDHs (GSAS-II[16]); high temperature calcination of the LDH to form $CuO/MgAl_2O_4$; redox cycling between $CuO/MgAl_2O_4$ and $Cu_2O/MgAl_2O_4$.

fuel for oxygen carriers with low loadings of active materials, which impacts the operating and capital expenditures of the scaled-up process. In this work, the oxygen release capacity of the MMOs was increased by increasing the molar ratio of $Cu^{2+}:Mg^{2+}:Al^{3+}$ from 3:1:2 to 5:1:2. In our previous work, we found that increasing the co-precipitation pH from 9.5 to 11 produced denser LDH platelets and MMOs with higher crushing strengths than those produced at pH 9.5.[11] Therefore, the higher loading MMOs were co-precipitated at pH 9.5 and 11, to investigate the effects of synthesis pH and loading on the performance of MMOs over long-term redox cycling in an FBR.

## Methods

### Synthesis

The LDH precursors were synthesised via co-precipitation at constant pH. A 2 M metal nitrate solution was prepared by dissolving $Cu(NO_3)_2 \cdot 2.5H_2O$, $Al(NO_3)_3 \cdot 9H_2O$ and $Mg(NO_3)_2 \cdot 6H_2O$ in the desired ratios in de-ionised water (DI water). An alkaline solution was prepared by dissolving 1 M NaOH and 1 M $Na_2CO_3$ in DI water. The two solutions were co-added to a reaction beaker under constant stirring at 300 rpm. The precipitate was aged for 1 h at room temperature and washed until the conductivity measured below 50 $\mu S\ cm^{-1}$. The washed precipitate was dried for > 12 h at 60°C then calcined at 975°C for

6 h in air. The MMOs were then crushed and sieved into the desired particle size ranges.

The 3:1:2 Cu-Mg-Al MMOs used for kinetic analysis were prepared from LDHs synthesised at a pH of 11. Detailed material characterisation of the LDHs and MMOs is described elsewhere.[11] The CuO loading of the MMOs was increased by changing the molar ratio of $M^{2+}/M^{3+}$ cations in the LDH precursor structure to test the effectiveness of the LDH-MMO design strategy. Naturally occurring LDHs typically have a molar ratio of $M^{2+}/M^{3+}$ equal to 2 (e.g. Quintinite, $[Mg_4Al(OH)_{12}](CO_3) \cdot 3H_2O$), or 3 (e.g. Hydrotalcite, $[Mg_6Al_2(OH)_{12}](CO_3) \cdot 4H_2O$) due to the local ordering of $M^{2+}$ and $M^{3+}$ that prevents the formation of $M^{3+}$ clusters.[17] Therefore, LDHs with a target molar ratio of $M^{2+}/M^{3+}$ of 3 were prepared via co-precipitation at constant pH values of 9.5 and 11 using a metal nitrate solution containing a 5:1:2 molar ratio of $Cu^{2+}:Mg^{2+}:Al^{3+}$. The LDHs and MMOs are referred to in-text as 'material-molar ratio-pH, for example, the LDH synthesised at pH 11 using a 5:1:2 molar ratio of $Cu^{2+}:Mg^{2+}:Al^{3+}$ is referred to as LDH-512-11.

### Kinetics of oxygen release

A model developed to determine the pseudo-intrinsic kinetics of the reduction of $Fe_2O_3$ by CO using an FBR[14] and the kinetic parameters of CaO carbonation at elevated pressures[15] was modified to extract oxygen release kinetics of the MMO-312-11. The model

assumes (a) the oxygen carrier particles were spherical; (b) the gas concentrations within the particles were pseudo-steady state; (c) the kinetics are first order. The model is described in detail in the Supporting Information.

A laboratory-scale FBR was used to study the oxygen release kinetics of the MMO-312-11 at high temperatures (850–962°C). A detailed description of the reactor set-up and control program written in Agilent Vee has been published elsewhere.[14] The calculation of the minimum fluidisation velocity, $u_{mf}$, is shown in the Supporting Information. The dimensionless parameter $u/u_{mf}$ provides a useful comparison of the actual gas velocity, $u$, to the $u_{mf}$. A $u/u_{mf}$ of 5 was used for all kinetic experiments in the FBR, based on initial screening experiments shown in the Supplementary Information. The $N_2$ flow rates for each experiment are provided in Supporting Information Table S1.

In a typical experiment, 40 g of inert sand (300–425 $\mu$m) was added to create the fluidised bed. A two-point calibration was carried out using air and a 10 vol% $O_2/N_2$ calibration gas. Three inert cycles of oxygen release and oxygen storage (i.e., without the presence of oxygen carriers) were carried out to provide baseline gas concentration profiles.

On completion of the inert cycles, 0.5 g of the MMOs (300–425 $\mu$m) was added to the fluidised bed. The sample mass and particle size were chosen to minimise the effects of external mass transfer and intraparticle diffusion while maintaining a good signal-to-noise ratio. High gas flow rates were also used to improve the quality of gas mixing in the bed. The signal from the gas analyser was deconvoluted using a method described elsewhere.[18] The rate of reaction was determined from the molar fraction of oxygen during redox cycling ($y_{O_2,redox}$) and leaving the reactor during inert cycles ($y_{O_2,inert}$) using Eqn (1),

$$r' \left[ \frac{mol\,(O_2)}{g_{OC}\,s} \right] = \frac{y_{O_2,redox} - y_{O_2,inert}}{dt} \cdot \frac{\dot{v}_{g,out}}{m_{OC} \cdot v_m} \quad (1)$$

where $m_{OC}$ is the mass of oxygen carriers, $v_m$ is the molar volume of the gas at standard ambient temperature and pressure (SATP), and $\dot{v}_{g,out}$ is the volumetric flow rate of the gas leaving the reactor defined using Eqn (2),

$$\dot{v}_{g,out} = \frac{\dot{v}_{g,in}}{1 - y_{O2}} \quad (2)$$

where $\dot{v}_{g,in}$ is the volumetric flow rate of the gas entering the reactor. The conversion was calculated from the rate using Eqn (3),

$$X = \frac{MW\,(O_2)}{R_0} \int_{t_0}^{t} r' \quad (3)$$

where $MW(O_2)$ is the molecular mass of oxygen and $R_0$ is the oxygen release capacity determined by thermogravimetric analysis.

The maximum rate of reaction at each temperature interval was found using Eqn (1) and was used to determine the intrinsic rate constants using the model described in the Supporting Information.

## Long-term cycling in a thermogravimetric analyser

Thermogravimetric analysis was carried out in a Q5000 thermogravimetric analyser (TGA) (TA Instruments) to evaluate the chemical stability of the MMOs over extended redox cycling. In a typical experiment, 5 mg of the oxygen carriers were spread into a single layer in a platinum crucible and cycled for 100 redox cycles. The experiments were performed at 900°C under a total gas flow rate of 200 ml min$^{-1}$ SATP. The observed oxygen release capacity was calculated as the difference between the relative weights at the beginning and end of the oxygen release period.

## Long-term cycling in a fluidised bed reactor

The long-term mechanical and chemical stabilities of the MMOs were assessed using an FBR. In a typical experiment, 15 g of MMOs (300–425 $\mu$m) were added to an FBR and cycled for 100 redox cycles at 900°C. The reduction and oxidation durations were sufficient to allow full oxygen release and oxygen storage. The conversion profiles of the MMOs were calculated using Eqn (1–3). A constant gas flow rate of 2.74 L min$^{-1}$ was used for the long-term cycling experiments. The flow rate was calculated based on the envelope density ($\rho_p$) of the 312-MMO-11 (3000 kg m$^{-3}$). This corresponds to $u/u_{mf}$ of 5, 4 ($\rho_p = 2400$ kg m$^{-3}$), and 5.3 ($\rho_p = 3200$ kg m$^{-3}$) for the 312-MMO-11, 512-MMO-9.5 and 512-MMO-11, respectively.

## Material characterisation

Powder X-ray diffraction (XRD) analysis was carried out using an X'Pert PRO (PANalytical) using Cu-K$\alpha$
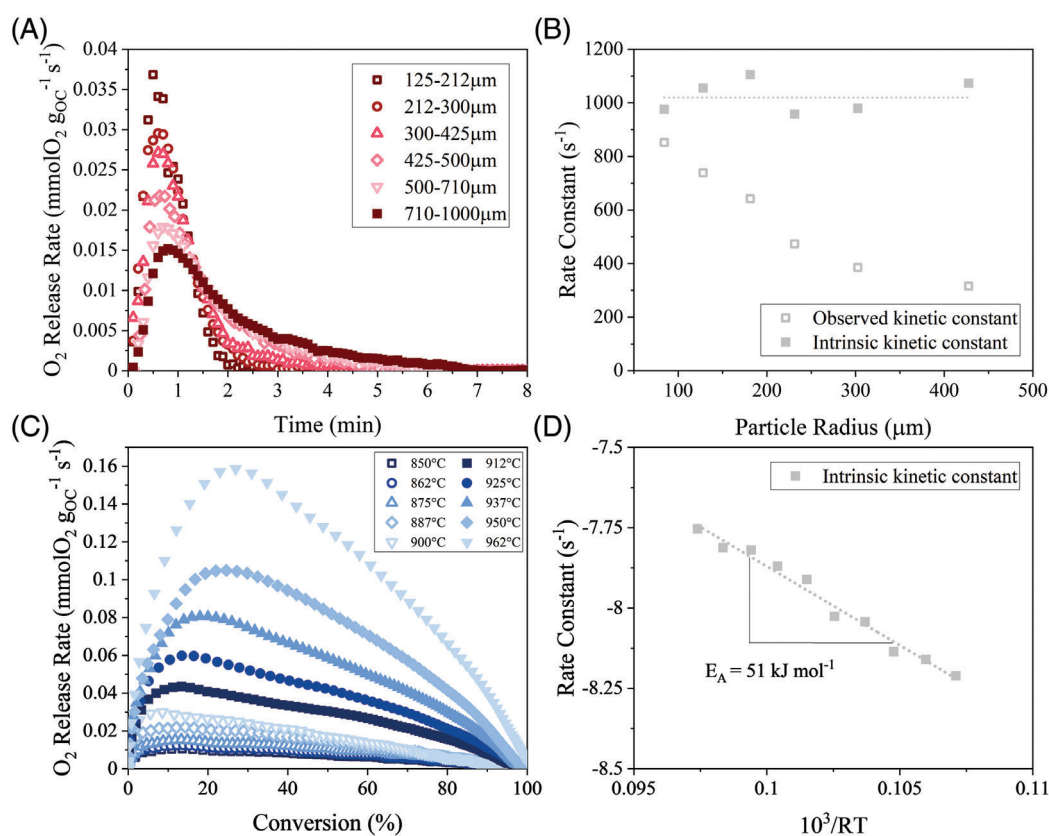
Figure 2. (A) rates of oxygen release for six particle size ranges using the averaged weight profile from cycles three to five in a TGA at 900°C (B) observed and fitted rate constants for average particle radii (C) rates of oxygen release of MMO-312-11 (300-425 $\mu$m) for the 850–962°C temperature range determined in an FBR (u/u$_{mf}$ = 5) (D) Arrhenius plot for the oxygen release of CuO to Cu$_2$O.

radiation ($\lambda$ = 0.1541 nm, 40 kV, 20 mA). X-ray fluorescence (XRF) was carried out using an Epsilon 3$^{XLE}$ spectrometer (PANalytical). Cu-Mg-Al oxides with eight different molar ratios were prepared via mechanical mixing to calibrate the XRF measurements. Mercury intrusion porosimetry (MIP) was carried out using an AutoPore IV 9500 (Micromeritics) to determine the pore volume between 10 nm and 10 $\mu$m. Helium pycnometry was carried out using an AccuPyc II 1340 (Micromeritics) to determine the skeletal density of the MMOs. The surface morphology of materials was studied using scanning electron microscopy (SEM) using an LEO Gemini 1525. The samples for SEM were coated with a thin layer of gold. The crushing strength was measured using a 50 N force gauge (Mark-10). The average crushing strength was determined from thirty measurements on single oxygen carrier particles (300–425 $\mu$m).

# Results and discussion

## Pseudo-intrinsic kinetics of 3:1:2 Cu-Mg-Al MMOs

The rate of oxygen release at 900°C is notably influenced by particle size, where six ranges of MMO-312-11 were considered (Fig. 2A). This influence can be considered by assessing the observed rate constant ($k_o$) and fitted intrinsic rate constant ($k_i$) (Fig. 2B). The value of $k_o$ can be seen to decrease with increasing particle radii due to increasing intraparticle mass transfer effects. Similarly, the effectiveness factors also decreased with increasing particle size fraction, as shown in Supplementary Table S2.

A particle size fraction of 300–425 $\mu$m was selected to study the intrinsic kinetics (kinetic model and FBR). This size fraction offers a trade-off between a reasonable effectiveness factor with both a good

**Table 1.  Results of kinetic studies of Cu-based oxygen carriers for CLOU processes, adapted from Xin et al.[26]**

| CuO loading (wt%) | Support | Reactor | Temperature (°C) | Kinetic Model* | $E_A$ (kJ mol$^{-1}$) | Reference |
|---|---|---|---|---|---|---|
| 18 | SiO$_2$ | TGA | 800–900 | NNGM (N = 2) | 315 | 27 |
|  |  |  | 900–975 |  | 176 |  |
| 20 | Al$_2$O$_3$ | FBR | 850–1100 | SCM | 81 | 28 |
| 40 | ZrO$_2$ | FBR | 900–985 | First order | 20 | 21 |
| 45 | ZrO$_2$ | TGA | 775–925 | First order | 58 | 20 |
| 50 | TiO$_2$ | TGA | 800–900 | First order | 67 | 20 |
| 60 | Al$_2$O$_3$-CaO | TGA, FBR | 850–950 | SCM | 60 | 19 |
| 60 | MgAl$_2$O$_4$ | TGA | 875–1000 | NNGM (N = 3/4) | 270 | 29 |
| 63 | MgAl$_2$O$_4$ | TGA, FBR | 850–962 | Effectiveness factor-based model | 51 | This work |
| 70 | SiO$_2$ | TGA | 700–900 | SCM | 249 | 30 |

*where NNGM is the nucleation and nuclei growth model; SCM is the shrinking core model

signal-to-noise ratio and low elutriation from the top of the FBR. The effectiveness factor was calculated to be 0.75 at 850°C and reduced to 0.62 at 962°C, indicating that intraparticle mass transfer effects were significant at higher temperatures (∼945°C) but were accounted for in the model.

The temperature dependence of $k_i$, modelled by the Arrhenius equation, (Eqn (4)) where: $E_A$ is the activation energy and $A$ is pre-exponential factor. The value of $k_i$ was recovered from the $k_o$ measured at each temperature by applying the effectiveness factor-based kinetic model. The Arrhenius plot (Fig. 2D) was used to extract $E_A$ of 51 ± 3 kJ mol$^{-1}$ and $A$ of 0.0567 s$^{-1}$ over the temperature range 850–962°C.

$$k_i = A \exp\left(\frac{E_A}{RT}\right) \qquad (4)$$

Table 1 summarises the results of kinetic analyses of Cu-based oxygen carriers published in literature. The activation energies vary significantly from 58 to 315 kJ mol$^{-1}$. The activation energy calculated in this work (51 kJ mol$^{-1}$) compares well with those measured by Hu et al.,[19] who reported an activation energy of 60 kJ mol$^{-1}$ using a TGA and FBR, and Clayton and Whitty who reported activation energies of 58 and 67 kJ mol$^{-1}$ for two different CuO-based oxygen carriers using a TGA.[20]

The oxygen carriers in Table 1 vary by loading of copper oxide, support material and particle size. The large spread of reported activation energies could be due to interactions between CuO and different support materials and mass transfer effects due to the choice of preparation method, particle size and other testing conditions, such as whether a TGA or FBR was used to produce the experimental data. Sahir et al. suggested that the high activation energies recorded in Table 1 are apparent activation energies which combine the thermodynamic driving force and true activation energy of the intrinsic kinetics.[21] The true activation energy may be found by subtracting the thermodynamic driving force, assumed to be equal to the standard enthalpy of oxygen release, ∼261 kJ mol$^{-1}$.[8]

## Synthesis of 5:1:2 Cu-Mg-Al LDH precursors and MMOs

The loading of active CuO in the MMOs was increased from 63 to 74 wt%; this was achieved by increasing the molar ratio of Cu$^{2+}$:Mg$^{2+}$:Al$^{3+}$ in the LDH precursor from 3:1:2 to 5:1:2. The 5:1:2 LDHs were synthesised *via* co-precipitation at two different pH values of 9.5 and 11 to investigate whether increasing the co-precipitation pH would result in LDHs and calcined MMOs with lower porosities, as observed previously
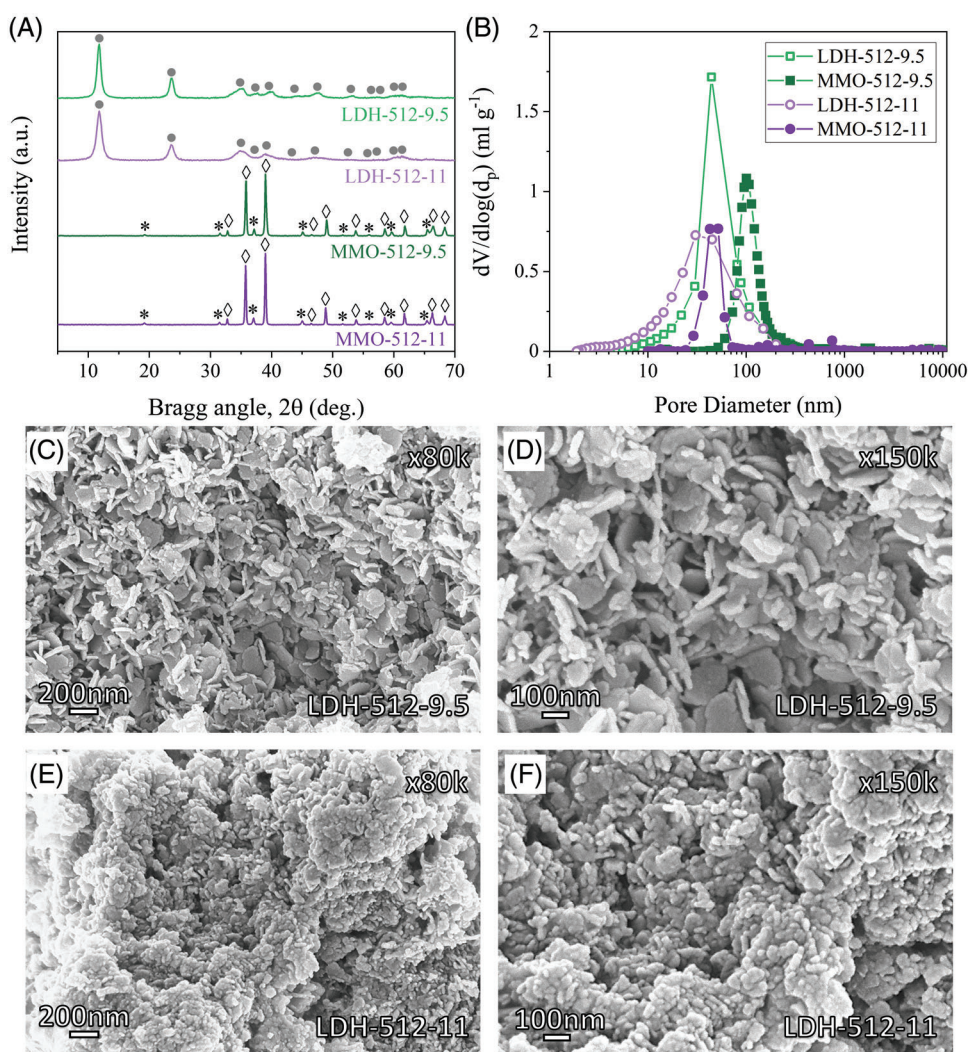
Figure 3. (A) XRD patterns of LDHs and MMOs, crystalline patterns correspond to ● $Mg_6Al_2(OH)_{16}CO_3\cdot4\,H_2O$ (JCPDS 22–0700), ◇ CuO (JCPDS 80–1268) and ∗ $MgAl_2O_4$ (JCPDS 73–1959); (B) $N_2$ adsorption and MIP pore size distributions of LDHs and MMOs; SEM images of LDH-512-9.5 particles at (C) 80k magnification and (D) 150k magnification; SEM images of LDH-512-11 particles at (E) 80k magnification and (F) 150k magnification

for LDHs with lower loadings of Cu.[11] From Fig. 3A, XRD analysis confirmed the formation of the LDH structure at both pH values and the formation of CuO and $MgAl_2O_4$ upon calcination. The content of Cu, Mg and Al in the MMOs was quantified using XRF; the target ratio of metals was achieved in the materials synthesised at each pH value (Supporting Table S3).

The pore size distributions and porosity of the LDHs and MMOs were probed using $N_2$ adsorption, MIP and helium pycnometry. The porosity of the LDH decreased from 64 to 47% when the pH was increased from 9.5 to 11. Imaging, using SEM, found the platelet size of the LDH was smaller for those produced at a higher pH (Fig. 3C–F). The smaller platelets aggregate into denser particles, as compared to those synthesised at pH 9.5. Upon high temperature calcination, the porosity decreased from 64 to 52% and 47 to 34% for the MMO-512-9.5 and MMO-512-11, respectively. The pore size distributions of the LDHs were found to shift toward larger pore diameters upon calcination to MMOs, likely due to the sintering of smaller pores (Fig. 3B). The average crushing strengths of the calcined particles were $1.7 \pm 1.0$ N and $4.5 \pm 1.6$ N for the MMO-512-9.5 and MMO-512-11, respectively.

An increase of co-precipitation pH from 9.5 to 11 resulted in LDHs and MMOs with lower porosities and
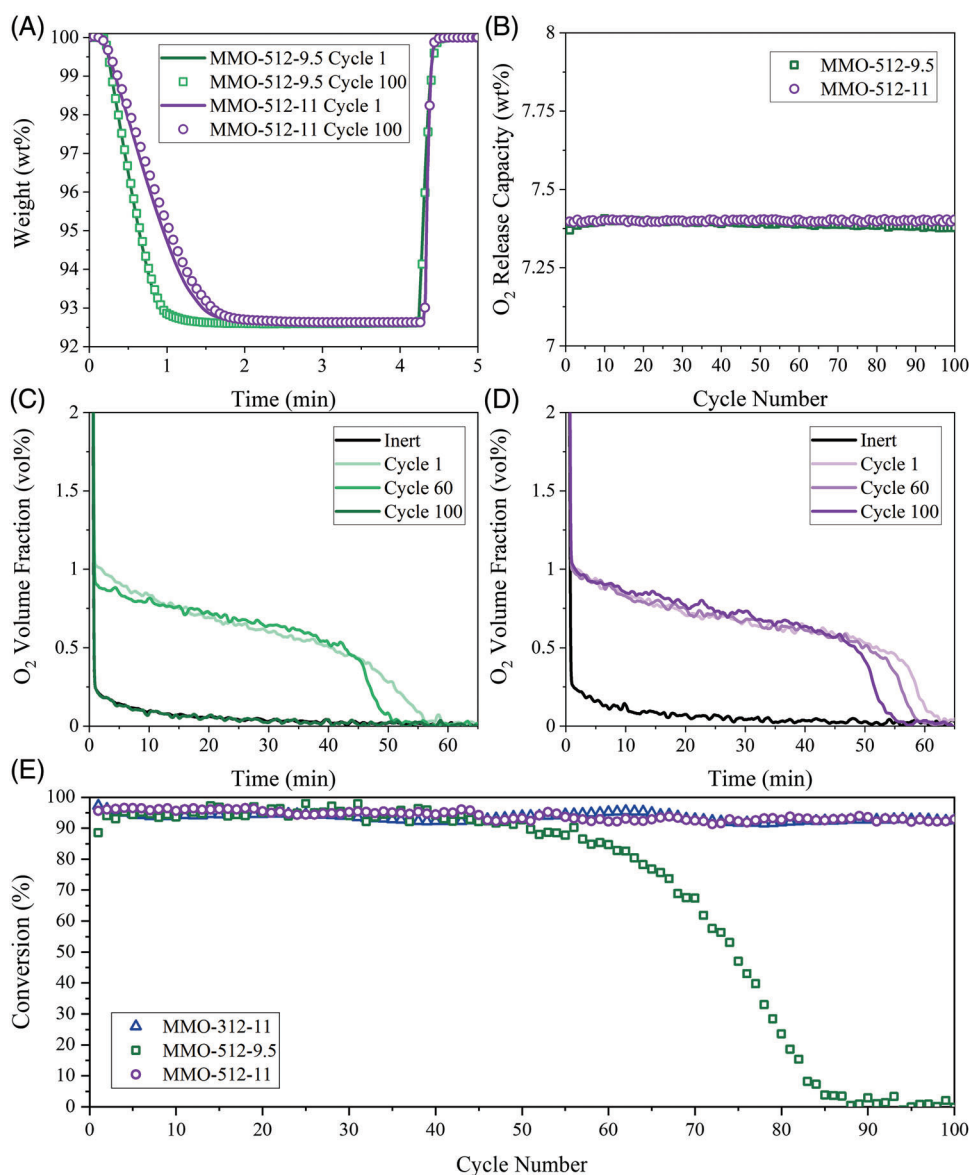
Figure 4. (A) oxygen release and storage profiles of the MMOs in a TGA at 900°C; (B) oxygen release capacities over 100 redox cycles in a TGA at 900°C; (c,d) oxygen release profiles for cycles 1, 60 and 100 in a FBR at 900°C for (C) MMO-512-9.5, note that the line for cycle 100 is superimposed on the inert signal, and (D) MMO-512-11; (E) conversion of MMO-312-11,[11] MMO-512-9.5 and MMO-512-11 over 100 cycles of full oxygen release and oxygen storage in a FBR at 900°C. A flow rate of 2.74 L min⁻¹ (SATP) was used for all experiments in the FBR.

MMOs with higher mechanical strength than those produced at pH 9.5 while maintaining the desired loading of CuO in the oxygen carrier.

## Long-term cycling of Cu-Mg-Al MMOs

Isothermal redox cycling was performed in a TGA to investigate the reactivity and stability of the MMOs. Figure 4A shows the first and last cycles of oxygen

release and storage profiles for the MMO-512s. The slower rate of decomposition of the MMO-512-11 compared to the MMO-512-9.5 (longer time required for total oxygen release) was attributed to the lower porosity of the MMO-512-11 and, therefore, lower intraparticle mass transfer effects. Both MMOs showed stable oxygen release capacities over 100 cycles, close to the theoretical capacity of 0.074 $g_{O2}/g_{MMO}$ (Fig. 4B).

The three largest pilot facilities for chemical looping processes use interconnected fluidised bed systems[22–24] where attrition of oxygen carriers is a significant barrier to commercialisation. While oxygen carriers undergoing redox reactions at high temperatures experience chemical and thermal stresses, which can induce structural changes due to sintering, the fluidised system inflicts additional physical stresses on the particle due to collisions with other particles and reactor walls, leading to particle breakage. To assess the mechanical stability of the materials, the MMOs were tested for 100 redox cycles in the FBR at 900°C.

The oxygen release profiles for cycles 1, 60 and 100 are shown in Fig. 4C–D. The overall conversion decreased from 94% to 0 over 88 cycles for the MMO-512-9.5, and 96 to 93% over 100 cycles for the MMO-512-11 (Fig. 4E). The observed decrease in conversion was due to severe attrition of the oxygen carriers during operation. The increased attrition of the MMO-512-9.5 compared to the MMO-512-11 is consistent with the higher porosity and lower crushing strength of the material. No agglomeration was observed in the MMO-512-11 samples withdrawn from the reactor after cycling. The conversion profile of the previously studied MMO-312-11 over 100 cycles in the FBR is shown in Fig. 4E. The LDH-MMO design strategy was effective at higher loading of active CuO, as demonstrated by the nearly constant conversion of MMO-512-11, comparable to the performance of MMO-312-11 in our previous work. The porosity and crushing strength of the MMO-312-11 were determined to be 38% and $5.7 \pm 2.6$ N, respectively, which are similar to the values obtained for the MMO-512-11. These results also indicate that the porosity of the material is a critical factor for oxygen carriers to withstand the mechanical stresses in the FBR. The CuO loading of these MMOs is much higher than the 13.8 wt% CuO oxygen carriers investigated in the EU-FP7 funded SUCCESS project (scale-up of oxygen carrier for chemical looping combustion using environmentally sustainable materials) so it could significantly reduce the required solids inventory for full fuel conversion.[25] The results indicate that Cu-Mg-Al MMOs are promising candidates for further development and scale-up for use in large scale fluidised chemical looping systems. Additional particle manufacturing techniques, such as spray drying, and optimisation of the calcination conditions could further improve the mechanical strength and attrition resistance of the oxygen carriers.

## Conclusion

This work demonstrated that the pseudo intrinsic kinetics of oxygen release from MMO-312-11s could be determined using an adapted effectiveness factor-based kinetic model to fit experimental data from an FBR. By modelling the internal and external mass transfer effects, the intrinsic rate constants for oxygen uncoupling were obtained for the temperature range 850–962°C. Using an Arrhenius expression, an activation energy of $51 \pm 3$ kJ mol$^{-1}$ and a pre-exponential factor of 0.0567 s$^{-1}$ were calculated for the oxygen release reaction. The activation energy reported in this work is similar to values reported in literature.

We also demonstrated the synthesis of Cu-Mg-Al LDH-derived MMOs with higher loadings of active CuO. High reactivity and excellent stability over extended redox cycling were observed using a TGA. We also found the structure and properties of the LDH precursors and derived MMOs could be effectively tailored by tuning the synthesis pH value. An increase in synthesis pH value changed the morphology of the LDH precursor and lowered the porosity of the material and derived MMOs, increasing the mechanical strength of the oxygen carriers. The near-constant conversion during long-term redox cycling experiments in an FBR at 900°C highlighted Cu-Mg-Al MMOs with high CuO loading as promising candidates for further development and scale-up.

## Acknowledgements

## References

1. Bui M, Adjiman CS, Bardow A, Anthony EJ, Boston A, Brown S et al. Carbon capture and storage (CCS): the way forward. Energy Environ Sci. 2018;11:1062–176.

2. Adanez J, Abad A, Garcia-Labiano F, Gayan P, De Diego LF. Progress in chemical-looping combustion and reforming technologies. Prog Energy Combust Sci. 2012;38:215–82.

3. Mattisson T, Lyngfelt A, Leion H. Chemical-looping with oxygen uncoupling for combustion of solid fuels. Int J Greenh Gas Control. 2009;3:11–19.

4. Patzschke CF, Boot-Handford ME, Song Q, Fennell PS. Co-precipitated Cu-Mn mixed metal oxides as oxygen carriers for chemical looping processes. Chem Eng J. 2021;407:127093.

5. Adánez-Rubio I, Gayán P, Abad A, de Diego LF, García-Labiano F, Adánez J. Evaluation of a spray-dried CuO/MgAl$_2$O$_4$ oxygen carrier for the chemical looping with oxygen uncoupling process. Energy Fuels. 2012;26: 3069–81.

6. Imtiaz Q, Kurlov A, Rupp JLM, Müller CR. Highly efficient oxygen-storage material with intrinsic coke resistance for chemical looping combustion-based CO$_2$ capture. ChemSusChem. 2015;8:2055–65.

7. Arjmand M, Azad A-M, Leion H, Mattisson T, Lyngfelt A. Evaluation of CuAl2O4 as an oxygen carrier in chemical-looping combustion. Ind Eng Chem Res. 2012;51:13924–34.

8. Jacob KT and Alcock CB. Thermodynamics of CuAlO$_2$ and CuAl$_2$O$_4$ and phase equilibria in the system Cu$_2$O-CuO-Al$_2$O$_3$. J Am Ceram Soc. 1975;58:192–5.

9. Chuang SY, Dennis JS, Hayhurst AN, Scott SA. Development and performance of Cu-based oxygen carriers for chemical-looping combustion. Combust Flame. 2008;154:109–21.

10. Arjmand M, Azad A-M, Leion H, Lyngfelt A, Mattisson T. Prospects of Al$_2$O$_3$ and MgAl$_2$O$_4$-supported CuO Oxygen carriers in chemical-looping combustion (CLC) and chemical-looping with oxygen uncoupling (CLOU). Energy Fuels. 2011;25:5493–502.

11. High M, Patzschke CF, Zheng L, Zeng D, Gavalda-Diaz O, Ding N et al. Precursor engineering of hydrotalcite-derived redox sorbents for reversible and stable thermochemical oxygen storage. Nat Commun. 2022;13:5109.

12. High M, Patzschke CF, Zheng L, Zeng D, Xiao R, Fennell PS et al. Hydrotalcite-derived copper-based oxygen carrier materials for efficient chemical-looping combustion of solid fuels with CO$_2$ capture. Energy Fuels. 2022;36: 11062–76.

13. Song Q, Liu W, Bohn CD, Harper RN, Sivaniah E, Scott SA et al. A high performance oxygen storage material for chemical looping processes with CO$_2$ capture. Energy Environ Sci. 2013;6:288–98.

14. Zhang Z, Hills TP, Scott SA, Fennell PS. Spouted bed reactor for kinetic measurements of reduction of Fe$_2$O$_3$in a CO$_2$/CO atmosphere part I:atmospheric pressure measurements and equipment commissioning. Chem Eng Res Des. 2016;114:307–20.

15. Fan Y, Yao JG, Zhang Z, Sceats M, Zhuo Y, Li L et al. Pressurized calcium looping in the presence of steam in a spout-fluidized-bed reactor with DFT analysis. Fuel Process Technol. 2018;169:24–41.

16. Toby BH and Von Dreele RB. GSAS-II: the genesis of a modern open-source all purpose crystallography software package. J Appl Crystallogr. 2013;46:544–9.

17. Mills SJ, Christy AG, Génin J-MR, Kameda T, Colombo F. Nomenclature of the hydrotalcite supergroup: natural layered double hydroxides. Mineral Mag. 2012;76:1289–336.

18. Fennell PS, Dennis JS, Hayhurst AN. The order with respect to oxygen and the activation energy for the burning of an anthracitic char in O2 in a fluidised bed, as measured using a rapid analyser for CO and CO$_2$. Proc Combust Inst. 2009;32:2051–8.

19. Hu W, Donat F, Scott SA, Dennis JS. Kinetics of oxygen uncoupling of a copper based oxygen carrier. Appl Energy. 2016;161:92–100.

20. Clayton CK and Whitty KJ. Measurement and modeling of decomposition kinetics for copper oxide-based chemical looping with oxygen uncoupling. Appl Energy. 2014;116:416–23.

21. Sahir AH, Sohn HY, Leion H, Lighty JS. Rate analysis of chemical-looping with oxygen uncoupling (CLOU) for solid fuels. Energy Fuels. 2012;26(7):4395–404. https://doi.org/10.1021/ef300452p.

22. Chiu J, Andrus H. Alstom's chemical looping technology program update. In: Proceedings of the 2014 national energy technology CO$_2$ capture technology meeting. Pittsburgh, PA. 2013.

23. Staničić I, Cañete Vela I, Backman R, Maric J, Cao Y, Mattisson T. Fate of lead, copper, zinc and antimony during chemical looping gasification of automotive shredder residue. Fuel. 2021;302:121147.

24. Ströhle J, Orth M, Epple B. Design and operation of a 1MWth chemical looping plant. Appl Energy. 2014;113:1490–5.

25. Penthor S, Mattisson T, Adánez J, Bertolin S, Masi E, Larring Y et al. The EU-FP7 Project SUCCESS – scale-up of oxygen carrier for chemical looping combustion using environmentally sustainable materials. Energy Procedia. 2017;114:395–406.

26. Tian X, Su M, Zhao H. Kinetics of redox reactions of CuO@TiO$_2$–Al$_2$O$_3$ for chemical looping combustion and chemical looping with oxygen uncoupling. Combust Flame. 2020;213:255–67.

27. Song H, Shah K, Doroodchi E, Wall T, Moghtaderi B. Analysis on chemical reaction kinetics of CuO/SiO$_2$ oxygen carriers for chemical looping air separation. Energy Fuels. 2014;28:173–82.

28. Means NC, Burgess WA, Howard BH, Smith MW, Wang P, Shekhawat D. Examining and modeling oxygen uncoupling kinetics of Cu-based oxygen carriers for chemical looping with oxygen uncoupling (CLOU) in a drop tube fluidized bed reactor. Energy Fuels. 2019;33:5610–9.

29. Adánez-Rubio I, Gayán P, Abad A, García-Labiano F, de Diego LF, Adánez J. Kinetic analysis of a Cu-based oxygen carrier: Relevance of temperature and oxygen partial pressure on reduction and oxidation reactions rates in chemical looping with oxygen uncoupling (CLOU). Chem Eng J. 2014;256:69–84.

30. San Pio MA, Martini M, Gallucci F, Roghair I, van Sint Annaland M. Kinetics of CuO/SiO$_2$ and CuO/Al$_2$O$_3$oxygen carriers for chemical looping combustion. Chem Eng Sci. 2018;175:56–71.

**Michael High**

Michael High is a PhD candidate in the Department of Chemical Engineering at Imperial College London. His research focuses on the development of synthesis-structure-performance relationships of oxygen carriers derived from structured precursors for chemical looping applications for $CO_2$ capture.
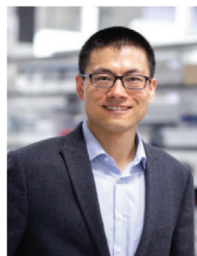
**Qilei Song**

Dr Qilei Song is a senior lecturer (associate professor) in the Department of Chemical Engineering at Imperial College London and one of the principal investigators at the Barrer Centre. He established the Functional Membrane and Energy Materials Group, and his research has broad applications in molecular separations, catalysis, and energy conversion and storage.

**Kyra Sedransk Campbell**

Dr Kyra Sedransk Campbell, PhD in Chemical Engineering, is a senior lecturer at the University of Sheffield working on materials degradation and decomposition. Her research operates at the interface of chemical engineering, materials science and chemistry studying the fundamentals that drive the changes that occur in dynamic, multiphase systems.

**Paul S. Fennell**

Professor Paul S. Fennell is a professor in the Department of Chemical Engineering at Imperial College London. His research focuses on clean energy production, including hybrid processes for co-production of hydrogen and valuable materials (steel, cement, chemicals), integration of different industries for decarbonisation, among other related areas.